Langmuir

Article

pubs.acs.org/Langmuir

Solvothermal Synthesis of Zincblende and Wurtzite $CuInS_2$ Nanocrystals and Their Photovoltaic Application

Wan-Chen Huang,[†] Chih-Hsiao Tseng,[†] Shu-Hao Chang,[‡] Hsing-Yu Tuan,[‡] Chien-Chih Chiang,[§] Lian-Ming Lyu,[†] and Michael H. Huang*[,†]

[†]Department of Chemistry, and [‡]Department of Chemical Engineering, National Tsing Hua University, Hsinchu 30013, Taiwan
[§]Green Energy and Environment Research Laboratories, Industrial Technology Research Institute, Hsinchu 31040, Taiwan

Supporting Information

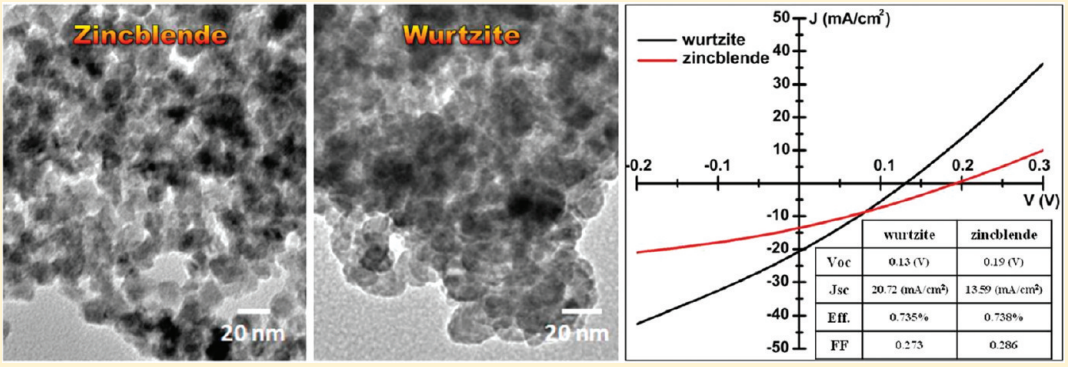

ABSTRACT: We report a simple solvothermal synthesis approach to the growth of $CuInS_2$ nanocrystals with zincblende- and wurtzite-phase structures. Zincblende nanocrystals with particle sizes of 10−20 nm were produced using oleylamine as the solvent. When ethylenediamine was used as the solvent, similarly sized wurtzite nanocrystals with some degree of particle aggregation were formed. Use of a mixture of these solvents gave products with mixed phases including some polyhedral nanostructures. The crystal phases of these nanocrystals were carefully determined by X-ray diffraction and transmission electron microscopy analysis. All the samples exhibit strong absorption from the entire visible light region to the near-infrared region beyond 1300 nm. Pure-phase zincblende and wurtzite $CuInS_2$ nanocrystals were employed as ink in the fabrication of solar cells. The spray-coated nanocrystal layer was subjected to a selenization process. A power conversion efficiency of ∼0.74% and a good external quantum efficiency profile over broad wavelengths have been measured. The results demonstrate that wurtzite and zincblende $CuInS_2$ nanocrystals may be attractive precursors to light-absorbing materials for making efficient photovoltaic devices.

INTRODUCTION

Copper indium sulfide/selenide (CIS) materials are known to have large light absorption coefficients in the visible light range and excellent stability under solar radiation and have been incorporated into the fabrication of solar cells as the light-absorbing layer.[1,2] Thin-film deposition using separate Cu, In, and S/Se sources has previously been employed to form this layer. Due to the high fabrication cost and composition uniformity problem associated with this film formation process, there is an increasing interest to use an ink process to generate the CIS layer.[3−8] Another important research direction involves the growth of monodisperse CIS and copper indium gallium sulfide/selenide (CIGS) nanocrystals for their potential applications in photovoltaic devices.[5−14] Most of the synthesized nanocrystals possess a tetragonal chalcopyrite crystal structure. $CuInS_2$ is one of the most promising light absorbers with a band gap of 1.45−1.5 eV, which is well matched with the solar spectrum.[15] Lu and co-workers reported the synthesis of first composition-tunable Cu−In−S nanocrystals with zincblende and wurtzite structures.[16] Here the zincblende phase has the same cubic sphalerite structure as ZnS, but with disordered occupancy of Cu and In cations. Cation positions are also random in wurtzite $CuInS_2$.[16] Since then, a number of studies have reported the synthesis of wurtzite and zincblende $CuInS_2$ nanocrystals.[15−20] Recently, wurtzite $CuInSe_2$ and $CuIn_xGa_{1-x}S_2$ nanocrystals have also been prepared.[21,22] The reaction temperatures were generally above 170 °C. Many of the synthesized wurtzite $CuInS_2$ nanocrystals have rather large platelike and irregular structures. Such features are not desirable as sources for the formation of thin films in photovoltaic devices; film thickness and smoothness can be more difficult to control. Furthermore, the use of novel wurtzite and zincblende $CuInS_2$ nanocrystals in the fabrication of solar cells has not been demonstrated before.

Received: February 21, 2012
Revised: May 1, 2012
Published: May 18, 2012

Table 1. Respective Solvent Volumes (mL) Used in Samples A–E

	sample A	sample B	sample C	sample D	sample E
oleylamine vol	14.0	10.5	7.0	3.5	0
ethylenediamine vol	0	3.5	7.0	10.5	14.0

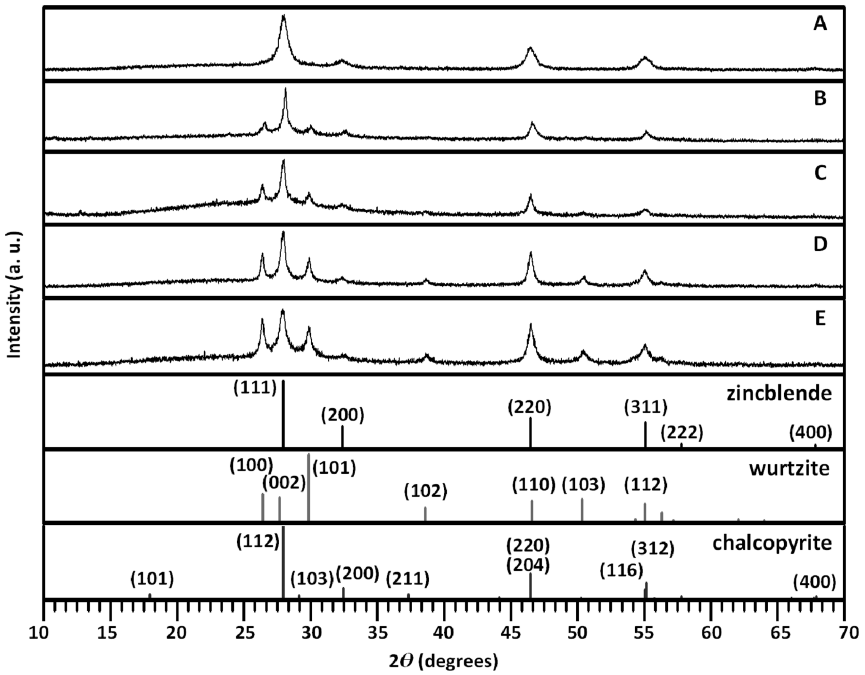

Figure 1. XRD patterns of the synthesized $CuInS_2$ nanocrystals in samples A–E. Simulated diffraction patterns of zincblende and wurtzite phases are also given.

In this study, we have successfully synthesized zincblende and wurtzite $CuInS_2$ nanocrystals with sizes of largely 10–20 nm by a simple solvothermal synthesis approach at a relatively low temperature of 160 °C. By using either oleylamine or ethylenediamine as the solvent, pure-phase products can be obtained. Use of a mixture of these solvents resulted in the production of nanocrystals with mixed wurtzite and zincblende phases. Because of their strong light absorption over the visible and near-infrared range and good size homogeneity, the zincblende and wurtzite $CuInS_2$ nanocrystals were applied in the fabrication of solar cells, converted in a selenization process, and then employed as the light-absorbing layer. A solar energy conversion efficiency of ∼0.74% has been recorded.

EXPERIMENTAL SECTION

Chemicals. Anhydrous copper chloride ($CuCl_2$; Riedel-de Haën, 97%), indium chloride ($InCl_3{\cdot}xH_2O$; Aldrich, 99.99%), thioacetamide (Fluka, 99%), oleylamine (Aldrich, 70%), ethylenediamine (Aldrich, 99%), and absolute ethanol (Aldrich, 99.9%) were used as received without further purification.

Synthesis of $CuInS_2$ Nanocrystals. In a typical synthesis of $CuInS_2$ nanocrystals, a stoichiometric mixture of $CuCl_2$ (0.0538 g, 0.4 mmol), $InCl_3{\cdot}xH_2O$ (0.0885 g, 0.4 mmol), and thioacetamide (0.0601 g, 0.8 mmol) was added to a 50 mL Teflon-lined autoclave. Subsequently 14 mL of oleylamine or ethylenediamine was introduced. Mixtures of oleylamine and ethylenediamine were also prepared and used for the nanocrystal synthesis (3.5, 7.0, and 10.5 mL of one component and the corresponding volumes of the other component for a total solvent volume of 14 mL). After the mixture was stirred for 10 s, the autoclave was sealed and transferred to an oven set at 160 °C for 12 h of reaction. Finally, the solution was naturally cooled to room temperature. The products were collected by centrifugation at 3000 rpm for 3 min. The precipitate was washed with absolute ethanol to remove excess solvent and unreacted reagents and redispersed in 3 mL of absolute ethanol for analysis.

Solar Cell Fabrication. Thin-film photovoltaic devices were fabricated with a conventional sandwich-type soda-lime glass/Mo/$CuInS_2$/CdS/ZnO/Al-doped ZnO (AZO) configuration. A Mo-coated soda-lime glass substrate was prepared by dc magnetron sputtering with a film thickness of 500 nm. A thick layer of $CuInS_2$ nanocrystals dispersed in absolute ethanol with a concentration of 20 mg/mL was evenly sprayed onto the Mo-coated glass substrate by using an airbrush (KUSING BD-130, 0.3 mm) operated at ∼20 psig of head pressure. Then the film was sintered at 400 °C in an Ar atmosphere for 1 h in a quartz tube to remove the solvent and other organic species, followed by selenization in an Ar and Se atmosphere at 550 °C for 40 min. A CdS buffer layer with a thickness of 80 nm was formed by chemical bath deposition using a solution containing 183 mL of deionized water, 25 mL of 0.015 M $CdSO_4$ solution, 12.5 mL of 1.5 M thiourea solution, and 31.25 mL of stock NH_4OH solution. Next a thin 100 nm intrinsic ZnO film capped with a ∼500 nm high-conductivity AZO layer was deposited by radio frequency (rf) magnetron sputtering. The ZnO film was sputtered in Ar mixed with 10% O_2 at a sputtering pressure of 10 mTorr, while the AZO layer was sputtered without O_2 at a sputtering pressure of 1 mTorr. No intentional heating was applied here. After formation of the oxide layers, the substrate was divided to make many small-area devices, and colloidal silver paste was applied to each cell as a top contact. The active area of each device is 0.14–0.15 cm^2.

Instrumentation. Scanning electron microscopy (SEM) images were acquired using a JEOL JSM-7000F scanning electron microscope. Transmission electron microscopy (TEM) characterization was performed on a JEOL JEM-2100 electron microscope operating at 200 kV. X-ray diffraction (XRD) patterns were collected using a Shimadzu XRD-6000 diffractometer with Cu Kα radiation. UV–vis absorption spectra were acquired with the use of a JASCO V-570

dx.doi.org/10.1021/la300742p | Langmuir 2012, 28, 8496–8501

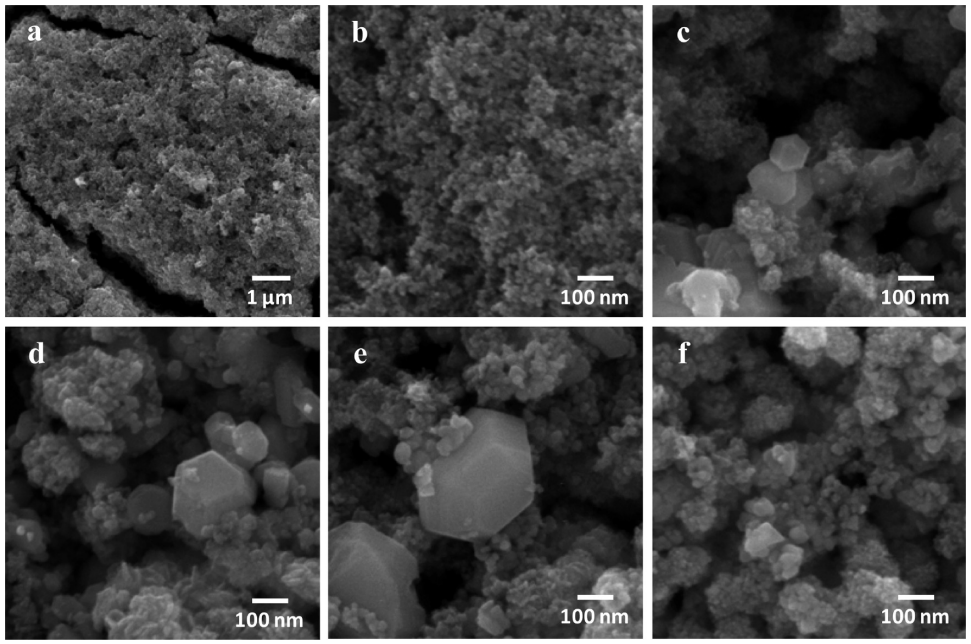

Figure 2. SEM images of the as-prepared $CuInS_2$ nanocrystals in sample (a, b) A at different magnifications, (c) B, (d) C, (e) D, and (f) E under the solvothermal condition at 160 °C for 12 h.

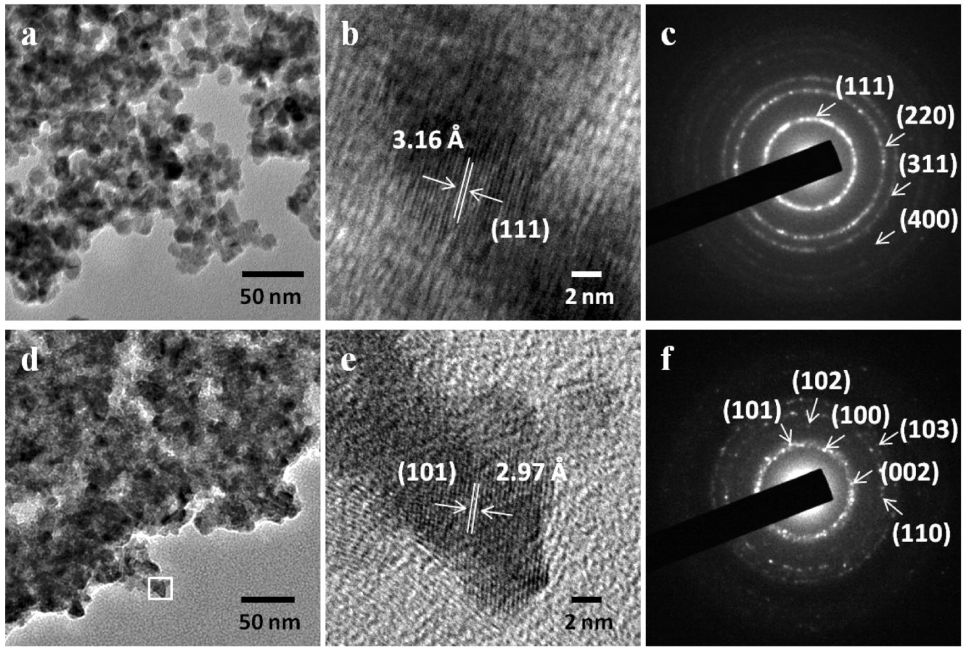

Figure 3. TEM images, high-resolution TEM images, and the corresponding SAED patterns of the (a–c) zincblende and (d–f) wurtzite $CuInS_2$ nanocrystals in samples A and E, respectively. Panel e shows the high-resolution TEM images of the square region in panel d. The concentric ring patterns recorded in SAED patterns indicate the polycrystalline nature of the products.

spectrophotometer. The *J*–*V* curves were obtained using a xenon lamp solar simulator under simulated AM 1.5 illumination (Continuous Solar Simulator for PV Cells, Hong-Ming Technology). The external quantum efficiency (EQE) was acquired with the use of an EQE measurement system from Hong-Ming Technology.

RESULTS AND DISCUSSION

For the solvothermal synthesis of $CuInS_2$ nanocrystals, a stoichiometric mixture of $CuCl_2$, $InCl_3{\cdot}xH_2O$, and thioacetamide was added to a Teflon-lined autoclave, followed by the addition of 14 mL of oleylamine, ethylenediamine, or a mixture of the two solvents. The autoclave was heated to 160 °C for 12 h to yield a black $CuInS_2$ nanocrystal solution. Scheme S1 (Supporting Information) gives a schematic illustration of the synthetic procedure. Five samples were made with solvent volume conditions listed in Table 1. Crystal structures of the synthesized products were first confirmed by their XRD patterns (see Figure 1). A close analysis of the XRD patterns indicates that the nanocrystals do not possess a chalcopyrite structure, because the (101), (103), and (211) reflection peaks of chalcopyrite $CuInS_2$ are missing in sample A. We then simulated diffraction patterns using the lattice parameters

dx.doi.org/10.1021/la300742p | *Langmuir* 2012, 28, 8496–8501

previously reported for zincblende and wurtzite $CuInS_2$ and found a good match with our XRD patterns.[16] The zincblende phase has a unit cell parameter a of 5.523 Å, while the wurtzite phase has unit cell parameters a of 3.897 Å and c of 6.441 Å. Crystal structure models of these two phases are available in the Supporting Information (Figure S1). The XRD patterns show that zincblende $CuInS_2$ nanocrystals were synthesized by using oleylamine as the solvent (sample A), while wurtzite $CuInS_2$ nanocrystals were produced with the use of ethylenediamine as the solvent. A weak peak at $2\theta = 33.0°$ in the XRD pattern of sample E suggests the presence of a small fraction of zincblende-phase nanocrystals. Absence of (101) and (211) diffraction peaks and the diffraction rings in thier selected-area electron diffraction (SAED) pattern (see Figure 3) confirms that wurtzite−chalcopyrite polytypism observed in $CuInS_2$ nanodisks is not present in sample E.[23] This finding indicates that the different degrees of coordinating interactions of solvent with the cations are critical to the crystal phases of the resulting nanoparticles. Ethylenediamine is more likely to coordinate to metal ions, forming complexes. It has a low boiling point of 116 °C, so the reaction should proceed vigorously and the mixture may even be under a supercritical condition. On the other hand, oleylamine with its high boiling point of 348 °C and nonpolar nature should be far less coordinating to the metal ions. The reaction conditions are quite different in these solvents, leading to the formation of different crystal phases. It was interesting to see how mixtures of these solvents affect the product crystal structures. With increasing contents of oleylamine from samples D to B, the wurtzite phase gradually converts into the zincblende phase.

The morphologies of the as-prepared $CuInS_2$ nanocrystals were examined by SEM. Figure 2 presents the SEM images of the nanocrystals in samples A−E. A large amount of zincblende $CuInS_2$ nanocrystals was formed in sample A with uniform particle sizes of 10−20 nm. The wurtzite nanocrystals in sample E appear to be aggregates of nanoparticles of sizes similar to those of the zincblende phase. Remarkably, large hexagonal platelike polyhedra were observed in all samples with mixed solvents. Their shapes are suggestive of a wurtzite-phase structure. The energy-dispersive X-ray spectrum of the wurtzite nanocrystals in sample E matches well with the expected atomic percentages of Cu, In, and S for $CuInS_2$, while the zincblende nanocrystals give a higher copper atomic content (see Figure S2, Supporting Information). The higher copper atomic content may be related to a greater amount of unreacted $CuCl_2$ left on the particles after washing. A higher carbon peak for the zincblende nanocrystals is suggestive of the adherence of oleylamine to the particle surfaces along with unreacted $CuCl_2$.

Further structural characterization of the zincblende and wurtzite $CuInS_2$ nanocrystals was performed using TEM. Figure 3 show results of the TEM analysis. Additional SEM and TEM images of these two phases are provided in Figure S3 (Supporting Information). Individual zincblende nanocrystals are discernible, but they form partial linkages to neighboring nanocrystals. More extensive particle aggregation and fusion is evident for the wurtzite nanocrystals. Lattice fringes with a d spacing of 3.16 Å were measured for a zincblende nanocrystal, which should correspond to the (111) lattice planes of zincblende $CuInS_2$. The SAED pattern of the zincblende nanocrystals produces a ring pattern that can be indexed to the (111), (220), (311), (400), and other planes of the zincblende phase. Again the diffraction rings from the (101) and (211) reflections are missing, unambiguously confirming that the synthesized nanocrystals do not possess a chalcopyrite structure. For the wurtzite nanocrystals, a measured d spacing of 2.97 Å from the reflections of the (101) lattice planes is consistent with the particle structure. The SAED pattern of the aggregated wurtzite nanocrystals also agrees with their assigned crystal structure.

The large faceted nanocrystals seen in samples with mixed solvents were also examined by TEM characterization (see Figure S4, Supporting Information). Representative hexagonal and triangular platelike nanostructures were analyzed. Both nanostructures give SAED patterns that can be matched to the wurtzite structure of $CuInS_2$ and are indicative of the single-crystalline nature of the nanocrystals. Lattice fringes with a d spacing of 3.2 Å were measured for both nanostructures, which correspond to the (002) lattice planes of wurtzite $CuInS_2$.

UV−vis absorption spectra of samples A−E dispersed in ethanol were taken and are displayed in Figure 4. All the samples show strong absorption over the entire visible light spectrum and significant absorption into the near-infrared region. Absorbance values of 0.3 and higher were recorded even at 1300 nm. This broad absorption feature to 1300 nm is particularly desirable for solar cell applications as a wide range of the solar spectrum can be utilized. The spectral profile for the zincblende $CuInS_2$ nanocrystals is different from that of the other samples with wurtzite-phase materials. Sample B shows an intermediate absorption profile, while samples C−E have nearly the same absorption band feature. Figure S5 (Supporting Information) offers a plot of $(\alpha h\nu)^2$ vs $h\nu$ for the determination of the direct band gap value of the zincblende and wurtzite $CuInS_2$ nanocrystals. Band gap energies of 1.32 and 1.42 eV were found respectively for the zincblende and wurtzite $CuInS_2$ nanocrystals, which are smaller than the band gap value of 1.45−1.5 eV for the chalcopyrite phase.

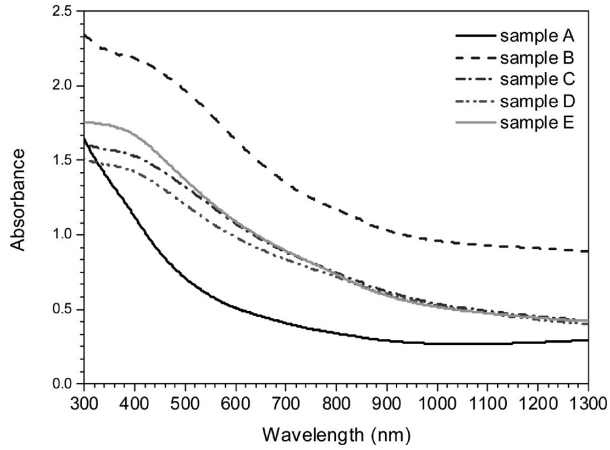

Figure 4. UV−vis absorption spectra of samples A−E.

With promising light absorption profiles into the near-infrared region, these $CuInS_2$ nanocrystals were fabricated into solar cells as the light-absorbing layer. Solar energy conversion efficiencies of the resulting photovoltaic devices were measured. The nanocrystal solutions from samples A and E were uniformly sprayed onto Mo-coated glass substrates (see Figure S6, Supporting Information), followed by thermal treatment at 400 °C and then selenization at 550 °C. The selenization process was found to be necessary because working devices were not fabricated without this process. However, by carefully tuning the cell fabrication process and possibly introducing a

dx.doi.org/10.1021/la300742p | Langmuir 2012, 28, 8496−8501

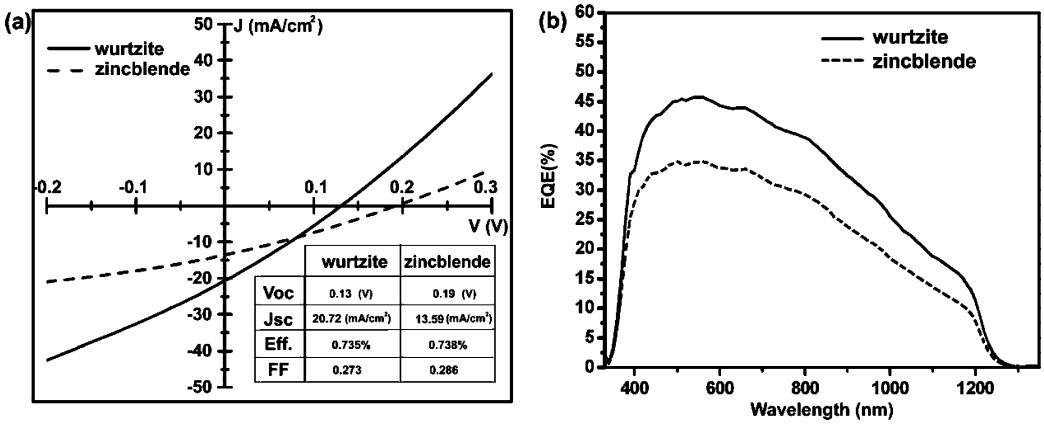

Figure 5. (a) $J-V$ curves and (b) EQE profiles of two completed solar cell devices using selenized wurtzite and zincblende $CuInS_2$ nanocrystals as the light-absorbing layer. Standard AM1.5 illumination was used.

suitable sulfur vapor source during the thermal treatment, it should be possible to obtain working solar cells without this selenization step. XRD patterns of the selenized zincblende and wurtzite nanocrystals reveal substitution of sulfur atoms with selenium atoms, and a chalcopyrite $CuInSe_2$ layer has been formed (see Figure S7, Supporting Information). It is believed that the high-temperature selenization process is favorable for the formation of a thermodynamically more stable chalcopyrite phase. Se atoms also diffused and reacted with the Mo back-contact during the selenization process, as evidenced by the appearance of $MoSe_2$ peaks in the XRD patterns. CdS, ZnO, and AZO layers were successively deposited on top of the absorber layer. The substrate was divided into many small-area devices, and a drop of silver paste was applied to form the top conductive contact. Figure S8 (Supporting Information) provides a top-view photograph of the final photovoltaic devices and a cross-sectional SEM image of a solar cell. The working area in each small cell is about 0.15 cm^2. The absorber layer was densely packed with a thickness of ~2.1 μm.

The $J-V$ characteristics of the solar cells and the corresponding EQE plots are shown in Figure 5. The best conversion efficiency measured for the selenized zincblende nanocrystals was 0.738% and that for the selenized wurtzite nanocrystals 0.735% with an active area of 0.14 cm^2 under AM 1.5 illumination. A large shunt leakage results in a lower open-circuit voltage (V_{oc}) and fill factor (FF). Even though solar cells fabricated using chalcopyrite $CuInS_2$ and $CuInSe_2$ nanocrystal ink have been reported to exhibit efficiencies of 2.15–4%, the purpose of this work is not to compare with or outperform their efficiency.[4,7,8] Instead, the purpose here is to examine the possibility of using novel zincblende and wurtzite $CuInS_2$ nanocrystals as ink for photovoltaic application. In this regard, this work represents the first attempt of such an investigation. It is worth noting that the first solar cells fabricated using chalcopyrite $CuInSe_2$ nanocrystal ink showed a power conversion efficiency of just 0.2%.[5] Thus, our measured efficiency is a good start for the two new phases of $CuInS_2$ nanocrystals. The EQE spectra for both devices show almost identical responses, exhibiting broad light-harvesting throughout the entire visible light region to ~1240 nm. The highest external quantum efficiency of 45% has been recorded for the wurtzite-based samples. The zincblende-based CIS solar cells present a lower integrated area, a result consistent with their lower short-circuit current (J_{sc}). The difference in EQE values for the two samples may be related to the solvent used to synthesize the nanocrystals. Carbon residue from residual oleylamine may be present after selenization for the zincblende nanocrystal sample due to the high boiling point of oleylamine. This may affect the charge transport and electrical resistivity in the film. The amount of carbon residue should be far less for the wurtzite-phase sample because of the low boiling point of ethylenediamine. However, similar EQE values for solar cells made from the zincblende nanocrystals have been measured, suggesting that improved EQE profiles can be obtained. It is expected that better conversion efficiency values should be achieved with optimized cell design and process conditions.

■ CONCLUSION

In summary, we have adopted a solvothermal synthesis approach to make $CuInS_2$ nanocrystals possessing zincblende and wurtzite crystal structures. Nanocrystals with a pure zincblende-phase structure were synthesized at 160 °C using oleylamine as the solvent. Wurtzite $CuInS_2$ nanocrystals were produced when the solvent was changed to ethylenediamine. Mixed zincblende and wurtzite nanocrystals resulted by mixing these solvents. The identity of these nanocrystals was carefully confirmed by XRD and TEM analysis. Both phases exhibit strong light absorption covering the entire visible light region to beyond 1300 nm. These nanocrystals were employed by spray-coating to fabricate working solar cells after selenization of the CIS absorber layer. A solar energy power conversion efficiency of ~0.74% and a good EQE profile over broad wavelengths have been measured, demonstrating the potential of zincblende and wurtzite $CuInS_2$ nanocrystals as attractive candidate precursors in the fabrication of photovoltaic devices.

■ ASSOCIATED CONTENT

Supporting Information

Scheme of the experimental procedure, crystal structures of different phases of $CuInS_2$, energy-dispersive X-ray spectra, additional SEM and TEM images of nanocrystals, $(\alpha h\nu)^2$ vs $h\nu$ plot, SEM image of the $CuInS_2$ nanocystal film, XRD patterns of selenized samples, photograph of the solar cells, and cross-sectional SEM image of a solar cell device. This material is available free of charge via the Internet at http://pubs.acs.org.

■ AUTHOR INFORMATION

Corresponding Author

*E-mail: hyhuang@mx.nthu.edu.tw.

dx.doi.org/10.1021/la300742p | *Langmuir* 2012, 28, 8496–8501

Notes

The authors declare no competing financial interest.

■ ACKNOWLEDGMENTS

We thank the National Science Council of Taiwan for financial support of this work (Grants NSC 98-2113-M-007-005-MY3, NSC 100-3113-E-007-009-CC2, and NSC 100-3113-E-007-008). C.-C.C. also appreciates financial support from the Department of Industrial Technology in the Ministry of Economic Affairs and Green Energy and Environment Research Laboratories, Industrial Technology Research Institute, Taiwan. Yu-Chen Yang's technical assistance in ink spraying and taking the cross-sectional SEM images is also acknowledged.

■ REFERENCES

(1) Klaer, J.; Bruns, J.; Henninger, R.; Siemer, K.; Klenk, R.; Ellmer, K.; Bräunig, D. Efficient $CuInS_2$ Thin-Film Solar Cells Prepared by a Sequential Process. *Semicond. Sci. Technol.* **1998**, *13*, 1456−1458.

(2) Lewerenz., H. J. Development of Copperindiumdisulfide into a Solar Material. *Sol. Energy Mater. Sol. Cells* **2004**, *83*, 395−407.

(3) Liu, W.; Mitzi, D. B.; Yuan, M.; Kellock, A. J.; Chey, S. J.; Gunawan, O. 12% Efficiency $CuIn(S,Se)_2$ Photovoltaic Device Prepared Using a Hydrazine Solution Process. *Chem. Mater.* **2010**, *22*, 1010−1014.

(4) Weil, B. D.; Connor, S. T.; Cui, Y. $CuInS_2$ Solar Cells by Air-Stable Ink Rolling. *J. Am. Chem. Soc.* **2010**, *132*, 6642−6643.

(5) Panthani, M. G.; Akhavan, V.; Goodfellow, B.; Schmidtke, J. P.; Dunn, L.; Dodabalapur, A.; Barbara, P. F.; Korgel, B. A. Synthesis of $CuInS_2$, $CuInSe_2$, and $Cu(In_xGa_{1-x})Se_2$ (CIGS) Nanocrystal "Inks" for Printable Photovoltaics. *J. Am. Chem. Soc.* **2008**, *130*, 16770−16777.

(6) Guo, Q.; Ford, G. M.; Hillhouse, H. W.; Agrawal, R. Sulfide Nanocrystal Inks for Dense $Cu(In_xGa_{1-x})(S_{1-y}Se_y)_2$ Absorber Films and Their Photovoltaic Performance. *Nano Lett.* **2009**, *9*, 3060−3065.

(7) Guo, Q.; Kim, S. J.; Kar, M.; Shafarman, W. N.; Birkmire, R. W.; Stach, E. A.; Agrawal, R.; Hillhouse, H. W. Development of $CuInSe_2$ Nanocrystal and Nanoring Inks for Low-Cost Solar Cells. *Nano Lett.* **2008**, *8*, 2982−2987.

(8) Li, L.; Coates, N.; Moses, D. Solution-Processed Inorganic Solar Cell Based on in Situ Synthesis and Film Deposition of $CuInS_2$ Nanocrystals. *J. Am. Chem. Soc.* **2010**, *132*, 22−23.

(9) Castro, S. L.; Bailey, S. G.; Raffaelle, R. P.; Banger, K. K.; Hepp, A. F. Synthesis and Characterization of Colloidal $CuInS_2$ Nanoparticles from a Molecular Single-Source Precursor. *J. Phys. Chem. B* **2004**, *108*, 12429−12435.

(10) Nairn, J. J.; Shapiro, P. J.; Twamley, B.; Pounds, T.; Wandruszka, R.; Fletcher, T. R.; Williams, M.; Wang, C.; Norton, M. G. Preparation of Ultrafine Chalcopyrite Nanoparticles via the Photochemical Deposition of Molecular Single-Source Precursors. *Nano Lett.* **2006**, *6*, 1218−1223.

(11) Xiao, J.; Xie, Y.; Xiong, Y.; Tang, R.; Qian, Y. A Mild Solvothermal Route to Chalcopyrite Quaternary Semiconductor $CuIn(Se_xS_{1-x})_2$ Nanocrystallites. *J. Mater. Chem.* **2001**, *11*, 1417−1420.

(12) Koo, B.; Patel, R. N.; Korgel, B. A. Synthesis of $CuInSe_2$ nanocrystals with Trigonal Pyramidal Shape. *J. Am. Chem. Soc.* **2009**, *131*, 3134−3135.

(13) Castro, S. L.; Bailey, S. G.; Raffaelle, R. P.; Banger, K. K.; Hepp, A. F. Nanocrystalline Chalcopyrite Materials ($CuInS_2$ and $CuInSe_2$) via Low-Temperature Pyrolysis of Molecular Single-Source Precursors. *Chem. Mater.* **2003**, *15*, 3142−3147.

(14) Zhong, H.; Zhou, Y.; Ye, M.; He, Y.; Ye, J.; He, C.; Yang, C.; Li, Y. Controlled Synthesis and Optical Properties of Colloidal Ternary Chalcogenide $CuInS_2$ Nanocrystals. *Chem. Mater.* **2008**, *20*, 6434−6443.

(15) Norako, M. E.; Franzman, M. A.; Brutchey, R. L. Growth Kinetics of Monodisperse Cu−In−S Nanocrystals Using a Dialkyl Disulfide Sulfur Source. *Chem. Mater.* **2009**, *21*, 4299−4304.

(16) Pan, D.; An, L.; Sun, Z.; Hou, W.; Yang, Y.; Yang, Z.; Lu, Y. Synthesis of Cu−In−S Ternary Nanocrystals with Tunable Structure and Composition. *J. Am. Chem. Soc.* **2008**, *130*, 5620−5621.

(17) Qi, Y.; Liu, Q.; Tang, K.; Liang, Z.; Ren, Z.; Liu, X. Synthesis and Characterization of Nanostructured Wurtzite $CuInS_2$: A New Cation Disordered Polymorph of $CuInS_2$. *J. Phys. Chem. C* **2009**, *113*, 3939−3944.

(18) Batabyal, S. K.; Tian, L.; Venkatram, N.; Ji, W.; Vittal, J. J. Phase-Selective Synthesis of $CuInS_2$ Nanocrystals. *J. Phys. Chem. C* **2009**, *113*, 15037−15042.

(19) Connor, S. T.; Hsu, C.-M.; Weil, B. D.; Aloni, S.; Cui, Y. Phase Transformation of Biphasic Cu_2S−$CuInS_2$ to Monophasic $CuInS_2$ Nanorods. *J. Am. Chem. Soc.* **2009**, *131*, 4962−4966.

(20) Bera, P.; Seok, S. I. Facile Synthesis of Nanocrystalline Wurtzite Cu−In−S by Amine-Assisted Decomposition of Precursors. *J. Solid State Chem.* **2010**, *183*, 1872−1877.

(21) Norako, M. E.; Brutchey, R. L. Synthesis of Metastable Wurtzite $CuInSe_2$ Nanocrystals. *Chem. Mater.* **2010**, *22*, 1613−1615.

(22) Wang, Y.-H. A.; Zhang, X.; Bao, N.; Lin, B.; Gupta, A. Synthesis of Shape-Controlled Monodisperse Wurtzite $CuIn_xGa_{1-x}S_2$ Semiconductor Nanocrystals with Tunable Band Gap. *J. Am. Chem. Soc.* **2011**, *133*, 11072−11075.

(23) Koo, B.; Patel, R. N.; Korgel, B. A. Wurtzite−Chalcopyrite Polytypism in $CuInS_2$ Nanodisks. *Chem. Mater.* **2009**, *21*, 1962−1966.